



# Numerical Investigation of Mixed Convection Heat Transfer in a Lid-Driven Cavity with Two Embedded Rotating Cylinders Based on Immersed Boundary-Lattice Boltzmann Method

Younes Farkach<sup>✉</sup>, Soufiane Derfoufi, and Mustapha Mahdaoui

ETTE, FSTT, Université de Abdelmalek Essaadi Tetouan, Tetouan, Morocco  
farkachyounes@gmail.com

**Abstract.** In this study, laminar mixed convection flow in a lid-driven cavity with two embedded rotating cylinders maintained at a hot temperature is examined. The upper wall of the enclosure is in motion and maintained at a cold temperature when the vertical walls are insulated. In this paper, the numerical method used is the lattice Boltzmann method (LBM). The numerical simulations are performed to investigate the Richardson number's effect on temperature/velocity fields and the rate of heat transfer. The immersed boundary method (IBM) is used to deal with the boundary conditions in complex geometries. It is found that for low Richardson number values, the natural convection mode is dominated by forced convection mode. In addition, increasing the Richardson number leads to a decrease in the rate of heat transfer.

**Keywords:** BGK-Lattice Boltzmann method · Mixed convection · Curved boundary · Lid-driven cavity

## 1 Introduction

The study of laminar mixed convection flow in the lid-driven cavity has been the interest among a number of engineering applications, such as cooling microelectronics devices, nuclear reactors, HVAC systems, food processing, and many others [1–6]. According to our bibliographic research, among the studies carried out in the context of this framework, we cite the numerical investigation of mixed convective heat transfer in a lid-driven cavity with rotating cylinders analyzed by Shubham et al.[7] for different Grashof numbers and various rotating speeds of the inner cylinders. Keya et al.[8] presented a numerical study of mixed convection inside a lid-driven enclosure with a double-pipe heat exchanger. The authors present the influence of several values of Richardson, Reynolds, and Prandtl numbers on heat transfer rate. They concluded that the rate of heat transfer is maximum for high values of  $Ri$  and  $Re$ , and low values of  $Pr$ . Another work recently published was fulfilled by Kashyap et al. [9], the authors used the lattice Boltzmann

method to investigate the influence of the cavity inclination on mixed convection in a two-sided lid-driven cavity with a hot porous block. They concluded that tilting the cavity increases the rate of heat transfer and entropy generation. The numerical study of MHD mixed convection in a lid-driven square enclosure filled with nanofluid was studied by Selimefendigil and Öztop [10] who used the Richardson and Hartmann numbers, cylinder’s angular rotational speed, and solid volume fraction of the nanoparticles as governing parameters.

To the best of our knowledge, no research have been carried out about laminar mixed convection flow in a lid-driven cavity with two rotating embedded cylinders and insulated vertical walls. In this study, we aim to use the lattice Boltzmann method with BGK approximation coupled with immersed boundary method (IBM) as a numerical tool to simulate laminar mixed convection in a lid-driven cavity with insulated vertical walls in the presence of two rotating hot cylinders. The governing parameters of this study are the Richardson number and different configurations related to the direction of rotation of the cylinders.

## 2 Problem Geometry and Numerical Method

### 2.1 Problem Geometry

Figure 1 presents the physical domain used in this work; it is composed of two inner cylinders of radii  $R_1$  and  $R_2$  inside a rectangular cavity. The two cylinders are uniformly heated to high temperature  $T_h$ , and the bottom and upper walls of the cavity are maintained at low temperature  $T_c$ , the vertical walls are insulated and air ( $Pr = 0.7$ ) is the working fluid.

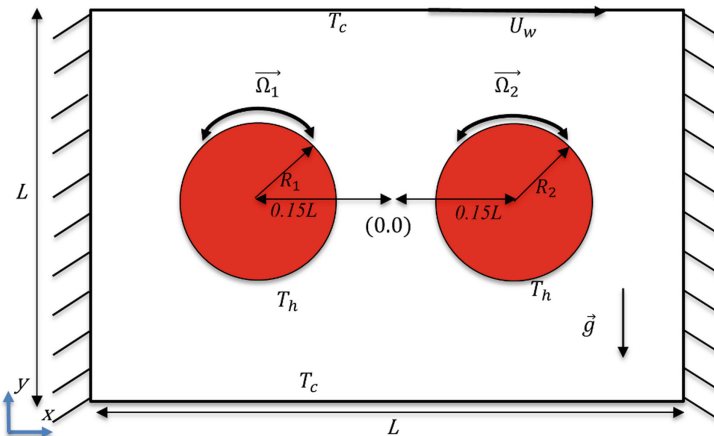


**Fig. 1.** Schematic diagram of the physical problem with boundary conditions

The Richardson number (Ri), Prandtl number (Pr), and Nusselt number ( $Nu_{av}$ ) are the dimensionless numbers taken into consideration in this study and are defined as:

$$Ri = \frac{Ra}{Re^2 Pr} \quad (1)$$

$$Nu_{av} = \frac{L}{(T_h - T_c)S} \int \frac{\partial T}{\partial n} ds \quad (2)$$

with S is the perimeter of the each cylinder, L is the characteristic length.  $Re$  and  $Ra$  refer to the Reynolds number and Rayleigh number respectively.

## 2.2 Numerical Method

In most cases, computational fluid dynamics (CFD), which is based on the Navier-Stokes equations, is used to simulate fluids behavior. Recently, the lattice Boltzmann approach stands out as an alternative to the conventional methods in the field of simulation of fluid flow and heat transfer. For this method, the fluid is presented by particles, which are located at lattice sites at time  $t$ , the particles are presented by a distribution function  $f$  and move in set directions as illustrated in Fig. 2.

The distribution functions are calculated by solving the Lattice Boltzmann Equation (LBE) (Eq. 3). Chen's simple relaxation time lattice Boltzmann method (SRT-LBM) [11] is adopted for this study.

$$\frac{\partial f}{\partial t} + c \cdot \Delta f = -\frac{1}{\tau_f} (f - f^{eq}) + F_{ext} \quad (3)$$

The parameter  $c$  is the particle velocity vector,  $f_i^{eq}$  the equilibrium distribution function,  $\tau_f$  represents the relaxation time and  $F_{ext}$  the external force term representing the buoyancy force  $F_{ext} = 3\omega_i g_y \beta \Delta T$  taking into consideration the Boussinesq approximation [12].

The discretized version of the LBE equation Eq. (3) is presented in Eq. (4);

$$\frac{\partial f_i}{\partial t} + c_i \cdot \Delta f_i = -\frac{1}{\tau_f} (f_i - f_i^{eq}) + F_{ext} \quad (4)$$

where  $i \in \{0,8\}$  and  $f_i$  stands the associated distribution function in direction  $i$ . This discretization conserves the mass, momentum, and energy of the fluid particles (conservation laws). The parameter  $c_i$  denotes the discrete velocity and  $f_i^{eq}$  the equilibrium distribution function.

The lattice-Boltzmann method solves Eq. (3) in two steps: collision and streaming.

- Collision:

$$f_i(x, t + \Delta t) = f_i(x, t) + \frac{\Delta t}{\tau_f} (f_i^{eq}(x, t) - f_i(x, t)) \quad (5)$$

- Streaming:

$$f_i(x + \Delta x, t + \Delta t) = f_i(x, t + \Delta t) \quad (6)$$

where  $\Delta t$  and  $\Delta x$  are the time step and lattice spacing, respectively.

According to [13], the equilibrium distribution function is represented in Eq. (7).

$$f_i^{eq} = \omega_i \left( 1 + \frac{3}{c^2} \mathbf{c}_i \cdot \mathbf{u} + \frac{9}{2c^4} (\mathbf{c}_i \cdot \mathbf{u})^2 - \frac{3}{2c^2} (\mathbf{u} \cdot \mathbf{u}) \right) \quad (7)$$

where  $\omega_i$  is the weight of the equilibrium distribution in the direction  $i$ .

$$\omega_{i=} \begin{cases} 4/9 & i = 0 \\ 1/9 & i = 1, 2, 3, 4 \\ 1/36 & i = 5, 6, 7, 8 \end{cases} \quad (8)$$

$$\mathbf{c}_{i=} \begin{cases} (0,0) & i = 0 \\ c \left( \cos\left(\frac{i-1}{2}\pi\right), \sin\left(\frac{i-1}{2}\pi\right) \right) & i = 1, 2, 3, 4 \\ c\sqrt{2} \left( \cos\left(\frac{2i-1}{4}\pi\right), \sin\left(\frac{2i-1}{4}\pi\right) \right) & i = 5, 6, 7, 8 \end{cases} \quad (9)$$

Equations (10) and (11) are used to calculate the macroscopic quantities such as fluid velocity and density.

$$\rho = \sum_{i=0}^{i=8} f_i \quad (10)$$

$$\rho \mathbf{u} = \sum_{i=0}^{i=8} \mathbf{c}_i f_i \quad (11)$$

The macroscopic temperature  $T$  is obtained by:

$$T(x, t) = \sum_{i=0}^{i=8} g_i(x, t) \quad (12)$$

where  $g_i$  are the internal energy distribution functions. In this study, the two-dimensional nine-velocity ( $D_2Q_9$ ) model is used for both density and energy distribution functions as shown in Fig. 2.

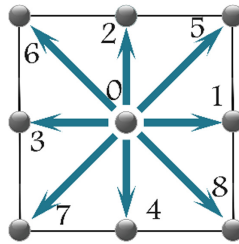


**Fig. 2.** The  $D_2Q_9$  model's lattice arrangement for 2D LBM.

### 2.3 Boundary Conditions

To deal with the boundary conditions, Guo et al. [14] propose the split-forcing method coupled with lattice-Boltzmann method to apply the effect of the immersed body force on a non-Newtonian flow field [15]. For this case, the density distribution function  $f_i$  and the internal energy density distribution  $g_i$  associated with the velocity and temperature fields are given respectively by:

$$f_i(x + \Delta x, t + \Delta t) = f_i(x, t) + \frac{\Delta t}{\tau_f} (f_i^{eq}(x, t) - f_i(x, t)) + F_i(x, t) \Delta t \quad (13)$$

$$g_i(x + \Delta x, t + \Delta t) = g_i(x, t) + \frac{\Delta t}{\tau_g} (g_i^{eq}(x, t) - g_i(x, t)) + Q_i(x, t) \Delta t \quad (14)$$

The quantities  $F_i(x, t)$  and  $Q_i(x, t)$  denote the discrete external force and the discrete energy source term, respectively, which are given by:

$$F_i(x, t) = \left(1 - \frac{1}{2\tau_f}\right) w_i \left(3 \frac{\mathbf{c}_i - \mathbf{u}(x, t)}{c^2} + 9 \frac{\mathbf{c}_i \mathbf{u}(x, t)}{c^4} \mathbf{c}_i\right) \cdot \mathbf{F}(x, t) \quad (15)$$

$$Q_i(x, t) = \left(1 - \frac{1}{2\tau_g}\right) w_i Q(x, t) \quad (16)$$

In the Eqs. (15) and (16), the terms  $\mathbf{F}(x, t)$  and  $Q(x, t)$  refer to the body force and energy source density, respectively. They are expressed by Eqs. (17) and (18) as follow:

$$\mathbf{F}(x, t) = 2\rho(x, t) \frac{U^d - U^{noF}(x, t)}{\Delta t} \quad (17)$$

where  $U^d$  is the desired velocity of the immersed boundary and  $U^{noF}(x, t)$  is the unforced velocity at the forcing point.

$$Q(x, t) = 2\rho(x, t) \frac{c^2}{3T_0} \frac{T^d - T^{noF}(x, t)}{\Delta t} \quad (18)$$

In the Eq. (18),  $T^d$  and  $T^{noF}(x, t)$  refer to the desired temperature of the immersed boundary and the unforced temperature at the interpolation point, respectively. It is to be noted that the steep boundary conditions given above are applied in the calculation algorithm between streaming and collision steps as referred in [16].

### 2.4 Code Validation

In order to validate the computer code, a verification has been carried out by comparing the results with certain results published in the literature in terms of isotherms and streamlines as illustrated in the Fig. 3.

A second validation has been carried out quantitatively in the case of free convection heat transfer generated between a heated imbedded cylinder and a square cavity studied by Shu et al. [18]. The comparative results presented in Table 1 in terms averaged values of Nusselt number  $\overline{Nu}$ , show a good agreement.

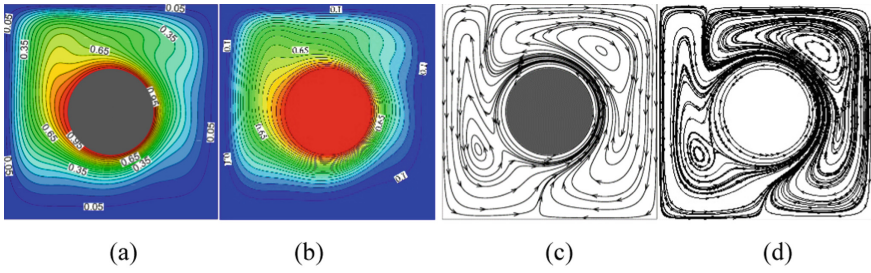


**Fig. 3.** Comparison of isotherms and streamlines with the results by Tao et al. [17] (a) and (c), and present work (b) and (d) respectively for  $Ri = 10$  and  $Pr = 0.7$ .

**Table 1.** Comparison of the average Nusselt number  $\overline{Nu}$  with previous results.

	$Ra = 10^4$	$Ra = 10^5$	$Ra = 10^6$
Shu et al. [18]	3.24	4.86	8.89
Present	3.34	4.82	8.86

### 3 Results and Discussion

To investigate the Richardson’s number effect for different rotational configurations of the cylinders on the isotherms and streamlines, the study is carried out using the grid  $200 \times 200$  for two values of the Richardson number ( $Ri = 0.5$  and  $100$ ), and four rotational configurations as indicated in Table 2.

**Table 2.** Configurations of rotational directions of the cylinders.

	Configuration 1	Configuration 2	Configuration 3	Configuration 4
Cylinder 1	Counter-clockwise	Counter-clockwise	Clockwise	Clockwise
Cylinder 2	Counter-clockwise	Clockwise	Counter-clockwise	Clockwise

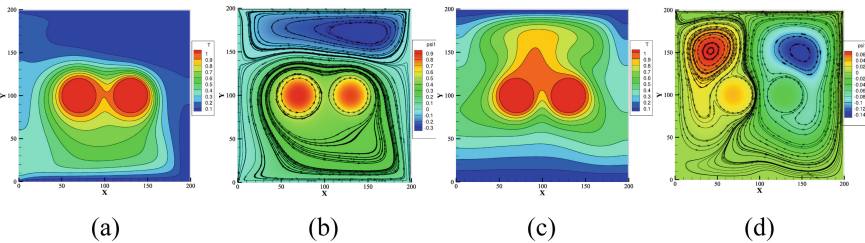


**Fig. 4.** Contours of isotherms (a)–(c) and streamlines (b)–(d) for  $Ri = 0.5$  (left) and  $Ri = 100$  (right) for the configuration 1.

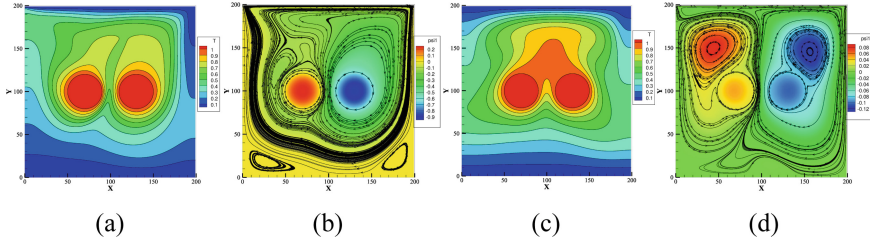


**Fig. 5.** Contours of isotherms (a)–(c) and streamlines (b)–(d) for  $Ri = 0.5$  (left) and  $Ri = 100$  (right) for the configuration 2.

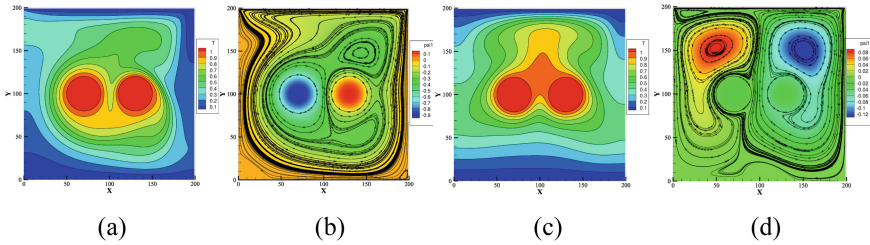


**Fig. 6.** Contours of isotherms (a)–(c) and streamlines (b)–(d) for  $Ri = 0.5$  (left) and  $Ri = 100$  (right) for the configuration 3.

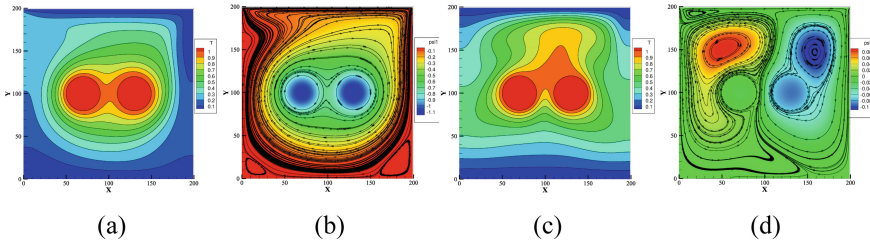


**Fig. 7.** Contours of isotherms (a)–(c) and streamlines (b)–(d) for  $Ri = 0.5$  (left) and  $Ri = 100$  (right) for the configuration 4.

The mixed convection flow in a lid-rectangular cavity with two embedded rotating hot cylinders is numerically carried out in this work. The impact of the Richardson number on the streamlines and isotherms is analyzed for two values of this parameter ( $Ri = 0.5$ ,  $Ri = 100$ ) and the four configurations as described in Table 2. It is to be remembered that the top wall of the cavity is moving at a constant velocity  $u_w$ .

Figures 4(c), 5(c), 6(c), and 7(c) illustrate the isotherms corresponding to  $Ri = 100$  for the four configurations. The appearance of the plume patterns in the isotherms indicates the dominance of the natural convection mode  $Ri \cdot Re \gg 1$ . In addition to that, the corresponding streamlines show complex structures generally dominated by two main cells. In the case of  $Ri = 0.5$ , illustrated in Figs. 4(a), 5(a), 6(a), and 7(a), the temperature field is strongly affected owing to the top wall motion and cylinders rotation,

which means that the magnitude of the forced convection becomes strong enough to affect the temperature field.

For the first configuration 1 (the two cylinders are counter-clockwise rotating). In Fig. 4(b), the flow structure at  $Ri = 0.5$  is characterized by the appearance of a large clockwise eddy in the upper part of the cavity, which prevents the appearance of the plume in the isotherms as in Fig. 4(c). Moreover, a large cell encompassing the cylinders and extending to the lower cold wall is formed. As a result, the thermal effect of the heating cylinders reaches the bottom zone of the cavity, whereas for  $Ri = 100$ , the corresponding isotherms illustrated in Fig. 4(d) show a cold zone in the lower part of the cavity and the area adjacent to the upper wall. This means that for  $Ri = 100$ , the effect of the heating cylinders is more apparent in the area above the cylinders due to the prevailing role of natural convection for this value of  $Ri$ .

Concerning configuration 2 (the cylinder 1 is counter-clockwise rotating and the cylinder 2 is clockwise rotating), the flow at  $Ri = 0.5$  consists of a large cell that covers the main part of the cavity and the inner cells formed around the rotating cylinders, as depicted in Fig. 5(b). This cell is due to the motion of the top wall of the cavity and supported the second cylinder that rotates clockwise. This configuration favors the appearance of two small vortices near the lower corners of the cavity and the extension of the zone heated by the cylinders above them even for this small value of  $Ri$  for which the shear force effect prevails.

The patterns of streamlines and isotherms corresponding to the configuration 3 (the first cylinder rotates clockwise and the second cylinder rotate counter-clockwise) are illustrated for  $Ri = 0.5$  and  $Ri = 100$  respectively in Fig. 6(a), (b), (c), (d). For this configuration where the two cylinders rotate in opposite directions, the aiding role between the moving wall and the left cylinder leads to a complex flow structure where the main formed cells rotate clockwise at  $Ri = 0.5$  as it can be seen in Fig. 6(b). The corresponding isotherms exemplified in Fig. 6(a) show the presence of a thermal plume pointing downward and an extension of the space affected by the heating of the cylinders up to the vicinity of the cold walls. At  $Ri = 100$ , the dominant effect of natural convection outweighs the forced convection, which favors the formation of two vertical cells around the cylinders (Fig. 6(d)) and modifies the orientation of the thermal plumes that all point upwards (Fig. 6(c)).

For the fourth configuration where the two cylinders rotate clockwise, the latter play an aiding role with the upper moving wall. Thus, at  $Ri = 0.5$ , the forced convection role is dominant and Figs.7(b) shows that the flow is mainly unicellular. The cell covers the whole space in the cavity and its inner lines surround the cylinders. As a result, the corresponding isotherms form contours enclosing the two cylinders while their open lines are mainly located in the areas not affected by the heating cylinders; i.e. near the cooled horizontal walls.

The results presented in Table 3 in terms of mean Nusselt number  $\overline{Nu}$ , show a better contribution of each cylinder to the heat transfer at  $Ri = 0.5$  for the configurations 1 to 3 since  $\overline{Nu}$  recorded at  $Ri = 100$  is noticeably lower for these configurations due to the fact that the mixed convection overcomes the natural convection. For the fourth configuration, the maximum stream function in Fig. 7(b) is located near the cavity wall, i.e. away from the two cylinders, which explains the exception of this configuration characterized by a



mean Nusselt number obtained with  $Ri = 100$  higher than that corresponding to  $Ri = 0.5$ .

**Table 3.** Average Nusselt number  $\overline{Nu}$  for both cylinders and all configurations.

$\overline{Nu}$	Configuration 1		Configuration 2		Configuration 3		Configuration 4	
	Ri = 0.5	Ri = 100	Ri = 0.5	Ri = 100	Ri = 0.5	Ri = 100	Ri = 0.5	Ri = 100
Cylinder 1	3.73	3.68	5.53	3.83	3.34	3.86	3.53	4.04
Cylinder 2	5.04	4.22	4.19	3.82	4.99	3.92	2.75	3.58

## 4 Conclusion

A numerical study of mixed convection heat transfer in lid-driven cavity with two embedded rotating cylinders and insulated vertical walls has been conducted. To achieve this problem, the immersed boundary-lattice Boltzmann based on the  $D_2Q_9$  model with the BGK collision operator was used. Four configurations corresponding to different rotational directions of the cylinders were considered. Based on the preliminary results, the forced convection mode prevails over natural convection at  $Ri = 0.5$ . In addition, the rate of heat exchange decrease was found globally attenuated by increasing the Richardson number for all configurations except the fourth one for which the tendency is reverted. These findings should be extended by considering more values of the governing parameters to arrive at more objective conclusions.

## Nomenclature

### Symbol, Name

$c_i$	Discrete lattice velocity in the direction $i$
$\mathbf{c}$	Microscopic velocity fluid particle
$f_i$	Distribution function of the velocity field
$f_i^{eq}$	Equilibrium distribution function of velocity field
$F_i$	External force
$g_i$	Distribution function of thermal field
$g_i^{eq}$	Equilibrium distribution function of thermal field
$g$	Gravitational acceleration
$L$	Characteristic length
$Pr$	Prandtl number $Pr = \frac{\eta}{\alpha}$
$Ra$	Rayleigh number $Ra = g\beta\Delta TL^3/\alpha\nu$
$Re$	Reynolds number $Re = \frac{U \times L}{\nu}$

Ri	Richardson number $Ri = \frac{Ra}{Re^2 Pr}$
T	Dimensionless temperature
T <sub>h</sub>	Hot temperature
T <sub>c</sub>	Cold temperature
T <sub>0</sub>	Reference temperature
U	Characteristic velocity
u, v	Vertical and horizontal components of velocity
$\mathbf{u} = (u, v)$	Macroscopic fluid velocity

### Greek Symbols

$\alpha$	Thermal diffusivity
$\beta$	Thermal expansion coefficient
$\Delta t$	Lattice time step
$\Delta x$	Lattice space step
$\omega_i$	Weighting factor in the direction i
$\rho$	Fluid density
$\vartheta$	Fluid viscosity
$\tau_f$	Flow relaxation time
$\tau_g$	Energy relaxation time

### Subscripts, Index

b	Boundary
c	Cold
eq	Equilibrium
h	Hot
i	Direction i
w	Wall
f	Density distribution function
g	Internal energy distribution function

### Abbreviations

BGK	Bhatnagar, Gross and Krook
CFD	Computational Fluid Dynamics
LBM	Lattice Boltzmann Method
SRT	Simple Relaxation Time

### References

1. Purusothaman, A.: Investigation of natural convection heat transfer performance of the QFN-PCB electronic module by using nanofluid for power electronics cooling applications. *Adv. Powder Technol.* **29**(4), 996–1004 (2018)

2. Ratzel, A.C., Hickox, C.E., Gartling, D.K.: Techniques for reducing thermal conduction and natural convection heat losses in annular receiver geometries (1979)
3. Iwatsu, R., Hyun, J.M., Kuwahara, K.: Mixed convection in a driven cavity with a stable vertical temperature gradient. *Int. J. Heat Mass Transf.* **36**(6), 1601–1608 (1993)
4. Msaad, A.A., et al.: Numerical simulation of thermal chaotic mixing in multiple rods rotating mixer. *Case Stud. Therm. Eng.* **10**, 388–398 (2017)
5. Farkach, Y., Derfoufi, S., Ahachad, M., Bahraoui, F., Mahdaoui, M.: Numerical investigation of natural convection in concentric cylinder partially heated based on MRT-lattice Boltzmann method. *Int. Commun. Heat Mass Transf.* **132**, 105856 (2022)
6. Derfoufi, S., Moufekkir, F., Mezhab, A.: Numerical assessment of the mixed convection and volumetric radiation in a vertical channel with MRT-LBM. *Int. J. Numer. Methods Heat Fluid Flow* (2018)
7. Dalvi, S., Bali, S., Nayka, D., Kale, S.H., Gohil, T.B.: Numerical study of mixed convective heat transfer in a lid-driven enclosure with rotating cylinders. *Heat Transf. Res.* **48**(4), 1180–1203 (2019)
8. Keya, S.T., Yeasmin, S., Rahman, M.M., Karim, M.F., Amin, M.R.: Mixed convection heat transfer in a lid-driven enclosure with a double-pipe heat exchanger. *Int. J. Thermofluids* **13**, 100131 (2022)
9. Kashyap, D., Dass, A.K.: Influence of cavity inclination on mixed convection in a double-sided lid-driven cavity with a centrally inserted hot porous block. *Int. J. Therm. Sci.* **181**, 107732 (2022)
10. Selimefendigil, F., Öztop, H.F.: Numerical study of MHD mixed convection in a nanofluid filled lid driven square enclosure with a rotating cylinder. *Int. J. Heat Mass Transf.* **78**, 741–754 (2014)
11. Chen, H., Chen, S., Matthaeus, W.H.: Recovery of the Navier-Stokes equations using a lattice-gas Boltzmann method. *Phys. Rev. A* **45**(8), R5339 (1992)
12. Boussinesq, J.: *Théorie analytique de la chaleur mise en harmonie avec la thermodynamique et avec la théorie mécanique de la lumière: Refroidissement et chauffage par rayonnement, conductibilité des tiges, lames et masses cristallines, courants de convection, théorie mécanique*, vol. 2. Gauthier-Villars (1903)
13. Girimaji, S.: *Lattice Boltzmann Method: Fundamentals and Engineering Applications with Computer Codes*. American Institute of Aeronautics and Astronautics (2013)
14. Guo, Z., Zheng, C., Shi, B.: Discrete lattice effects on the forcing term in the lattice Boltzmann method. *Phys. Rev. E* **65**(4), 46308 (2002)
15. Feng, Z.-G., Michaelides, E.E.: The immersed boundary-lattice Boltzmann method for solving fluid-particles interaction problems. *J. Comput. Phys.* **195**(2), 602–628 (2004)
16. Delouei, A.A., Nazari, M., Kayhani, M.H., Succi, S.: Immersed boundary—thermal lattice Boltzmann methods for non-Newtonian flows over a heated cylinder: a comparative study. *Commun. Comput. Phys.* **18**(2), 489–515 (2015)
17. Tao, S., He, Q., Chen, B., Qin, F.G.F.: Distribution function correction-based immersed boundary lattice Boltzmann method for thermal particle flows. *Comput. Part. Mech.* **8**(3), 459–469 (2021)
18. Shu, C., Xue, H., Zhu, Y.D.: Numerical study of natural convection in an eccentric annulus between a square outer cylinder and a circular inner cylinder using DQ method. *Int. J. Heat Mass Transf.* **44**(17), 3321–3333 (2001)